

Stages of neuronal network formation

Lydia Woiterski^{1,4}, Thomas Claudepierre², Robert Luxenhofer³,
Rainer Jordan³ and Josef A Käs¹

¹ Institut für Experimentelle Physik I, Abteilung Physik Weicher Materie,
Universität Leipzig, Linnéstraße 5, D-04103 Leipzig, Germany

² Klinik und Poliklinik für Augenheilkunde, Universitätsklinikum Leipzig,
Liebigstraße 10–14, D-04103 Leipzig, Germany

³ Professur für Makromolekulare Chemie, Department Chemie, Technische
Universität Dresden, Zellescher Weg 19, D-01069 Dresden, Germany

E-mail: lydia.woiterski@uni-leipzig.de

New Journal of Physics **15** (2013) 025029 (15pp)

Received 11 October 2012

Published 22 February 2013

Online at <http://www.njp.org/>

doi:10.1088/1367-2630/15/2/025029

Abstract. Graph theoretical approaches have become a powerful tool for investigating the architecture and dynamics of complex networks. The topology of network graphs revealed small-world properties for very different real systems among these neuronal networks. In this study, we observed the early development of mouse retinal ganglion cell (RGC) networks *in vitro* using time-lapse video microscopy. By means of a time-resolved graph theoretical analysis of the connectivity, shortest path length and the edge length, we were able to discover the different stages during the network formation. Starting from single cells, at the first stage neurons connected to each other ending up in a network with maximum complexity. In the further course, we observed a simplification of the network which manifested in a change of relevant network parameters such as the minimization of the path length. Moreover, we found that RGC networks self-organized as small-world networks at both stages; however, the optimization occurred only in the second stage.

 Online supplementary data available from stacks.iop.org/NJP/15/025029/mmedia

⁴ Author to whom any correspondence should be addressed.



Content from this work may be used under the terms of the [Creative Commons Attribution-NonCommercial-ShareAlike 3.0 licence](http://creativecommons.org/licenses/by-nc-sa/3.0/). Any further distribution of this work must maintain attribution to the author(s) and the title of the work, journal citation and DOI.

Contents

1. Introduction	2
2. Methods and materials	3
2.1. Preparation of lipidic substrates for neuronal growth	3
2.2. Immunoisolation and culture of primary neurons	4
2.3. Image acquisition	5
2.4. Data analysis	5
3. Results and discussion	6
3.1. Development of retinal ganglion cell networks	6
3.2. Quantification of network phases	8
3.3. Retinal ganglion cell networks are small-world networks	11
4. Concluding remarks	12
Acknowledgments	13
References	13

1. Introduction

Complex networks are ubiquitous—be it the internet, transportation networks, social networks or those of the family of biological networks such as protein, metabolic or neural networks. Stimulated by two pioneering works about small-world networks [1] and scale-free networks [2], interest in these networks has grown tremendously within the last two decades. Advances in the description of complex networks led to a resurgence of graph theoretical approaches which are a powerful tool for studying the network’s architecture and dynamics [3–7]. In neuroscience, this is reflected by numerous topology studies on wiring diagrams or connectomes reaching from the neural network of the nematode worm *Caenorhabditis elegans* (*C. elegans*) [1, 8] over neuronal networks grown *in vitro* [9, 10], networks of macaque and cat cerebral cortex [11–13] up to the human brain [14–16]. The nature of these networks is small—not in the sense of length scales, but in terms of the network class. While featuring high clustering coefficients similar to regular lattices, they exhibit short characteristic path lengths like random graphs [1]. In neural networks in particular, these two characteristics were shown to allow a high signal propagation speed combined with coherent oscillations [17].

The complexity of the brain manifests in the intricate relation of structural and functional networks which challenges researchers from many fields [4, 12, 15, 16, 18, 19]. Although to date it is not yet possible to predict the brain’s global functionality from the anatomical connectivity [20], a recent work proclaims auspicious progress in large-scale computational models that were used to relate functional brain dynamics and structural connectivity patterns [21]. To understand the principles of the structural organization in the early stage of neuronal network formation, it is convenient to study neuronal growth *in vitro* [9, 10, 22]. Shefi *et al* [22] described in detail the outgrowth behaviour and formation of locust frontal ganglion cell (FGC) networks. They observed increasing complexity with a maximum between 2 and 3 days *in vitro* followed by a simplification of the network after 1 week. In a second study, they characterized the morphological properties of clustered 6-day-old FGC networks and found that cultured neuronal networks exhibit small-world properties [9]. Recently, functional networks of

pre-natal rat dissociated cortical cultures on multi-electrode arrays were shown to develop from random networks (after 14 days *in vitro*) to small-world networks (after 4–5 weeks *in vitro*) [10]. Based on this, the authors extensively discussed the changes of the small-world parameters during network maturation and related them to activity changes such as reduced bursting times.

In this study, we investigated the formation of mouse retinal ganglion cell (RGC) networks *in vitro* using time-lapse video microscopy to understand how single cells self-organize towards small-world networks without external stimuli. *In vivo* RGCs alone never form networks but connect their dendritic arborization to bipolar and amacrine cell axons on the one side and form the optic nerve via fasciculation of long RGC axons on the other side [23]. Defasciculation and branching only occur when RGCs reach their targets in the brain. Thus, *in vivo* external signals (from glia cell precursors, surrounding neurons and guidance molecules) block the formation of the homologous connections between RGCs that we observe *in vitro*. From previous studies it is known that RGCs recover from the dissection and regrow neurites *in vitro* between 2 and 4 days after plating [24] and form two-dimensional (2D) networks *in vitro* as shown in [25]. Therefore, neurite outgrowth monitoring was started between 17 and 20 h after seeding the cells to ensure the observation, from the beginning, of the network development. The monitoring ended after 2 days in culture when connected networks had formed. Topological maps were abstracted from the phase contrast images using MATLAB to characterize the network properties. Graph theory was applied to determine the typical network parameters such as connectivity, shortest path length and clustering coefficient [4], as well as the edge length that is also referred to as wiring length [15]. In agreement with previous studies on neuronal networks, we found that RGC networks also belong to the small-world networks [3, 9]. Interestingly, the time-resolved graphical analysis of the evolving system revealed different stages during the course of network formation. To the author's knowledge, this is the first study where on the basis of graph theoretical analysis it could be shown how neuronal networks in a first stage form a highly complex small-world network which in the second stage self-optimizes to a network with reduced path lengths.

2. Methods and materials

2.1. Preparation of lipidic substrates for neuronal growth

In this study, primary neuronal cells were seeded on tethered lipid bilayers (tBLs) coated with extracellular matrix proteins. Firstly, these substrates reduce the effects of glass such as a higher surface charge. Secondly, *in vivo* neurons grow in close contact with other cells; therefore, tBLs better mimic the viscoelastic properties of cell membranes than a conventional glass cover slip. The tBLs were produced by Langmuir–Blodgett (LB)/Langmuir–Schaefer (LS) transfer. The phospholipid 1-palmitoyl-2-oleoyl-*sn*-glycero-3-phosphocholine (POPC) was purchased from Avanti Polar Lipids (Alabaster, AL). The lipopolymer 1,2-distearoyl-*sn*-glycerol-poly(2-methyl-2-oxazoline)₅₀ (PMOx₅₀) was synthesized as described previously [26, 27]. Analysis by gel permeation chromatography and MALDI-ToF mass spectrometry confirmed a monomodal distribution with a dispersity index of 1.2 and an average degree of polymerization of $n = 49$ –50. ¹H-NMR spectroscopy confirmed a quantitative functionalization of the polymer termini. Then, 1,2-distearoyl-*sn*-glycero-3-phosphoethanolamine-*N*-[succinimide ester (polyethylene glycol)-2000] (NHS-ester) was prepared by hydrogenation [28] of PEG2000-Maleimide by the group of C A Naumann. Round glass cover slips (4 cm; 631-0177, VWR

International, Dresden, Germany) were cleaned with a Hellmanex solution (Sigma Alridch, Schnellendorf, Germany) in a sonicating water bath at 40 °C for 60 min, rinsed extensively with Millipore water, hydrophilized in a plasma cleaner (Harrick, Ithaca, NY) for 2 min and stored until use in Millipore water (not longer than 2 days). For the inner leaflet, a mixture of POPC and 5 mol% PMO_{x50} dissolved in chloroform ($\geq 99\%$; Merck, Darmstadt, Germany) was spread on a Langmuir trough equipped with a Wilhelmy pressure detector and a dipper unit (Nima, Espoo, Finland) filled with Millipore water. The lipid monolayer was compressed to a surface pressure of 30 mN m⁻¹ (corresponding to an average area per lipid of 63 Å²) and allowed to stabilize for 20 min. The transfer to the glass cover slip was carried out with a dipping speed of 1 mm min⁻¹ to avoid lipid/lipopolymer phase separation during transfer [27, 29]. For using tBLs as cell substrates, the bottom part of a Petri dish with a cut-out 3 cm hole was deposited upside down on the bottom of the dipping unit's cavity. Moreover, a ring of vacuum grease was added around the Petri dish's hole for later sealing. After renewing the Millipore subphase, a solution of POPC and 5 mol% NHS-ester in chloroform was spread on the trough, compressed and allowed to equilibrate as before. The bilayer was completed by pushing the cover slip with the LB layer horizontally through the LS layer and sticking it on top of the Petri dish. The Petri dish was permanently kept in aqueous surroundings to maintain the tBL intact.

2.2. Immunoisolation and culture of primary neurons

Postnatal (P7) BALB/c mice from our animal facility were killed by decapitation according to institutional guidelines. Retinae were isolated and RGCs were purified by immunopanning as reported previously [24, 25]. Briefly, this technique is based on the specific expression of Thy1.2 protein at the surface of the sole RGC in the mouse retina. Using an antibody raised against the extracellular domain of the molecule it is possible to isolate this rare neuronal type from a retinal cell suspension. We could therefore analyse over time the change in network complexity directly and solely on these neurons without possible bias due to mixed culture use and uncontrolled release of factors from surrounding cells. Petri dishes with tBL substrates were twice carefully flushed with PBS (Gibco/Invitrogen, Karlsruhe, Germany) under sterile conditions and coated with laminin (1.42 $\mu\text{g cm}^{-2}$, Santa Cruz Biotechnology, Santa Cruz, CA) and merosin (0.71 $\mu\text{g cm}^{-2}$, Chemicon, Millipore, Billerica, MA). 80 000–150 000 RGCs were plated on each dish yielding a cell density of 110–200 cells mm⁻². The typical distance between cells ranged between 90 and 140 μm (on average (111 \pm 6) μm). RGCs were cultured at 37 °C, 5% CO₂, 95% humidity in Neurobasal medium (Gibco/Invitrogen, Karlsruhe, Germany) supplemented with (all from Sigma, except where indicated) pyruvate (1 mmol l⁻¹), glutamine (2 mmol l⁻¹; Gibco/Invitrogen), *N*-acetyl-L-cysteine (60 $\mu\text{g ml}^{-1}$), putrescine (16 $\mu\text{g ml}^{-1}$), selenite (40 ng ml⁻¹), bovine serum albumin (100 $\mu\text{g ml}^{-1}$; fraction V, crystalline grade), streptomycin (100 $\mu\text{g ml}^{-1}$), penicillin (100 U ml⁻¹), triiodothyronine (40 ng ml⁻¹), holotransferrin (100 $\mu\text{g ml}^{-1}$), dibutyryl cyclic AMP (250 $\mu\text{mol l}^{-1}$), insulin (5 $\mu\text{g ml}^{-1}$), progesterone (62 ng ml⁻¹), B27 (1:50, Gibco/Invitrogen), D-manose (50 $\mu\text{mol l}^{-1}$), brain-derived neurotrophic factor (BDNF; 25 ng ml⁻¹; PeproTech, London, GB), ciliary neurotrophic factor (CNTF; 10 ng ml⁻¹; PeproTech) and forskolin (10 $\mu\text{mol l}^{-1}$). Neurons were allowed to adhere and start the neurite outgrowth in the incubator overnight. For measurements, the Petri dish was placed in a custom-made heater to keep the RGCs at 37 °C and closed with a special Teflon top with two connections to apply a gentle flow of moistened synthetic air (Air Liquide, Düsseldorf, Germany) with 5% CO₂ over the medium in the dish. The medium was

not exchanged after plating the cells since primary neurons are very sensitive and would retract all their neurites during this procedure.

2.3. Image acquisition

Time-lapse phase contrast video microscopy was carried out using an inverted microscope (DMIRB) equipped with a motorized x–y-stage (DMSTC; both from Leica Microsystems, Wetzlar, Germany), an E-660 Piezo Driver (PI Physik Instrumente, Karlsruhe, Germany) for adjustment of the objective height, a custom-made heater and CO₂ supply. Images were taken every 3 or 5 min using an ORCA-285 IEEE 1394-based CCD camera (Hamamatsu Photonics Deutschland, Herrsching am Ammersee, Germany) with a 20 × NA0.40 objective (Leica Microsystems, Wetzlar, Germany) and 1 × C-mount. Automated image acquisition was done using the movable x–y-stage controlled by a LabVIEW (National Instruments, Austin, TX) routine to record long-term image series of neuronal networks at ten different positions of the same Petri dish. The measurements were started 17–20 h after plating to ensure that neurites had started growing out, and were ended after 38–41 h when the networks were optimized.

2.4. Data analysis

A fully automated tracking of nodes and edges was not possible here, because to date there is no standard method for extracting neurite morphology combined with the connectivity information from phase contrast imaging data. However, ongoing progress in the reconstruction of neuronal branching [30, 31], as well as improvements in the analysis and comparison of structural and functional brain networks [6, 32], makes it a highly active area of research. In this study, topological mapping of the RGC networks was carried out using the *Adjacency Matrix GUI* [33] from MATLAB (MathWorks, Natick, MA), which allows defining nodes and their interconnections and returns the adjacency matrix. Furthermore, it was modified to also determine the coordinates of the nodes for the edge length analysis. In accord with Shefi *et al* [9], we considered neurons, synapses, the large growth cones (at the leading edge as well as those growing out of the soma) and all branching points as vertices of the network (see figure 1). To find real nodes and connections, in ambiguous cases, previous and successive image frames were considered. In the time course of the network formation, the cells showed ageing, first reflected by an enhanced occurrence of neuronal beading, i.e. the formation of bulbous structures, after neurite retraction. Nevertheless, the cells were still viable as they continued growing out neurites with large growth cones and many filopodia. Secondly, some connections became thinner and finally vanished. Those were included as long as there was still visible transport along the corresponding neurite.

For the generated graphs, we assumed all vertices and edges between the vertices to be identical and disregarded multiple connections between two vertices [9]. The resulting graphs are undirected and unweighted. Let v_1, v_2, \dots, v_n be the vertices of the graph abstracted from the neuronal network images. Then the adjacency matrix $A = a_{ij}$ of order n , which characterizes the graph, is symmetric and given by [34]

$$a_{ij} = \begin{cases} 1 & \text{if } v_i \text{ and } v_j \text{ are directly connected by an edge,} \\ 0 & \text{otherwise.} \end{cases}$$

The temporal evolution of network topology was examined by setting up the adjacency matrices A in time steps of 90 min. The node connectivity is given by the degree k of a vertex

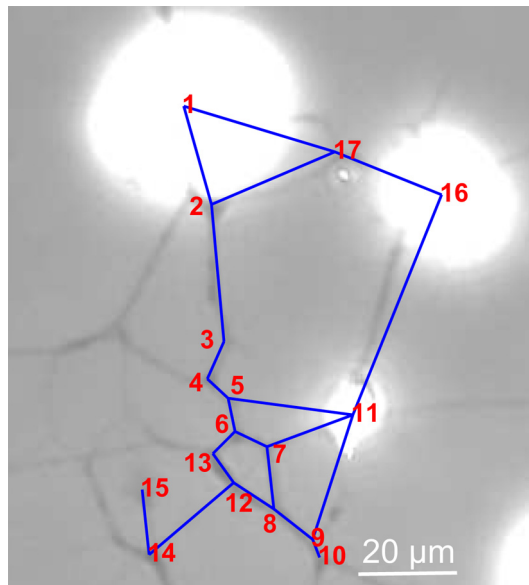


Figure 1. Illustration of the topological mapping for a small section of an RGC network. Somata, synapses and all branching points are defined as vertices (red numbers). Two neighbouring vertices are connected by an edge as depicted by the blue lines.

v_i , i.e. the number of all other directly connected vertices. It was determined from A by simple algebraic manipulations as described previously [9]. Two important parameters that characterize the network type are the shortest path length L between a pair of vertices v_i and v_j and the clustering coefficient C_v which describes the cliquishness of a neighbourhood [1]. The shortest path length L is defined as the minimum number of edges which has to be traversed from v_i to v_j . If the vertex v has k_v neighbours, the maximal possible number of edges between its neighbours is given by $k_v(k_v - 1)/2$. Then, the clustering coefficient C_v is defined as the actual number of edges between the k_v neighbours divided by the maximal possible number. L and C_v were calculated from the adjacency matrix using available MATLAB routines [33, 35]. Since the path length does not correspond to a physical length, the edge length d , i.e. the Euclidean distance between a pair of vertices v_i and v_j , was also determined.

3. Results and discussion

3.1. Development of retinal ganglion cell networks

Neuritogenesis of RGCs cultured on tBLs was observed starting 17–20 h after seeding. Figure 2 shows the development of an RGC neuronal network at four different stages. At the beginning, isolated RGCs showed neurites, while small networks were rarely observed. Extending neurites initiated branching and formed connections to other cells which thereby got activated and formed new outgrowths. We did not observe self-avoidance of neuronal connections, i.e. neurites connected to outgrowths of one and the same cell. ‘Activation’ of most of the cells occurred approximately up to 19–23 h *in vitro*. With ongoing time, the cells formed new processes which sometimes followed the path of already existing neurites before branching

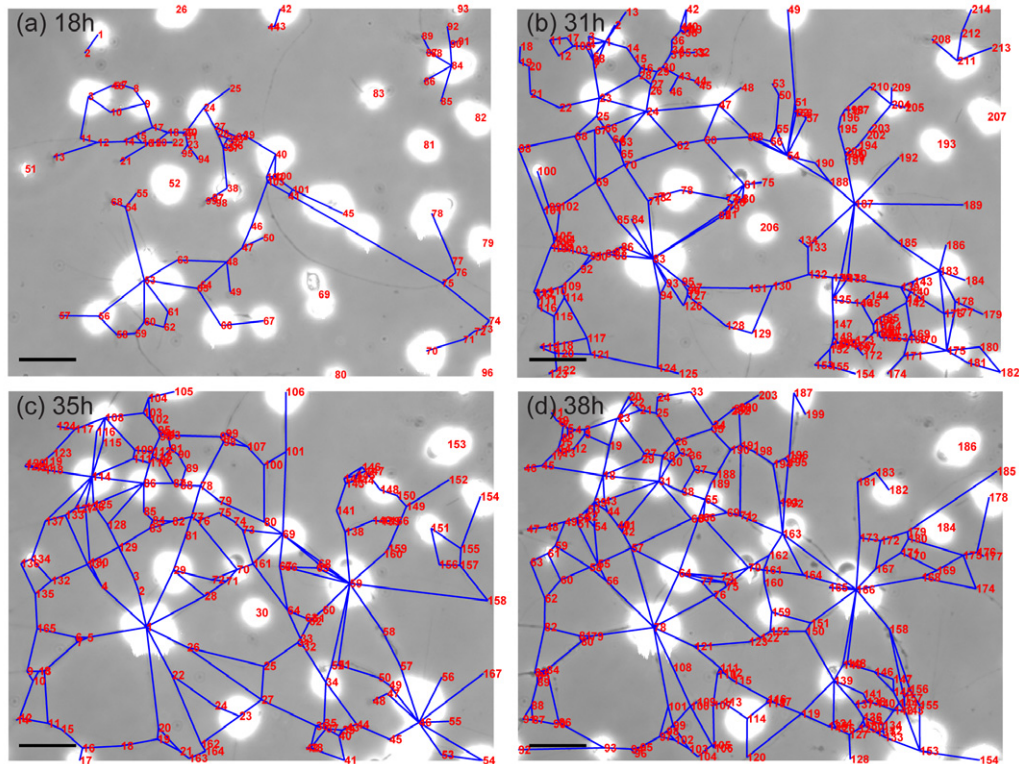


Figure 2. Development of an RGC network. The phase contrast images and overlaid topological graphs show the network (a) when starting the observation at 18 h *in vitro*, (b) at the maximum complexity (31 h), (c) after the optimization (35 h) and (d) at the end of the observation (38 h). Vertices are marked by red numbers, existing connections by blue edges. Scale bars correspond to 50 μm . The cell density was 202 cells mm^{-2} . (The entire image series is provided in the supplementary data, available at <http://stacks.iop.org/NJP/15/025029/mmedia>.)

again. Thus, the network got more elaborate by the formation of further connections to existing neurites or other cells (including multiple connections between two neighbouring cells) until reaching a maximal complexity (figure 2(b)). At that stage, the network displayed a high level of arborization and many short neurite segments. During the entire observation, neurites kept growing out and formed further connections. However, after reaching the maximum complexity, the dominant effect was an optimization of the network. The reduction occurred by the fusion of parallel neurites to strengthened bundles, the weakening or removal of neurites as well as the clustering of cells by migration of somata along a connection (figure 2(c)). Moreover, we observed a straightening out of neurites. This outgrowth behaviour of RGCs *in vitro* was found to be similar to that reported for 2D cultures of locust FGCs by Shefi *et al* [9]; however, mouse RGC networks develop faster. In this study, mouse RGCs exhibited a maximum complexity after 30–36 h *in vitro* in contrast to 3 days for locust FGCs. Also optimized networks appeared earlier, i.e. between 36 and 41 h *in vitro* (4–5 days for locust FGCs) [22]. Towards later stages of our measurements (35–41 h), some networks underwent enhanced neuronal beading and ageing of neurites which influenced the network’s reduction process and could not be distinguished from ‘real’ optimization. Nevertheless, the RGCs were still viable (see section 2.4) and showed the same behaviour as neurons without neuronal beading.

Table 1. Mean values and SEMs for the number of vertices, the number of edges and the number of non-connected cells (averaged over 13 networks resulting from three cell preparations).

	Start	Maximum network	Optimized network
Vertices	52 ± 6	142 ± 21	112 ± 17
Edges	40 ± 8	175 ± 31	143 ± 27
Non-connected cells	13 ± 2	5 ± 1	4 ± 1

Already simple parameters indicate distinct properties of the neuronal network at different temporal stages. In contrast to the beginning, maximum networks exhibited much larger numbers of vertices and connections (table 1). Further, the number of non-connected cells decreased drastically. For optimized networks, both the average number of connections as well as the average number of vertices dropped by approximately 20%.

Another feature of the networks is that not all neurons were in the same stage at the same time. A closer look at the centre of figure 2(b) reveals maximum complexity of the network as reflected by the high density of vertices. In figure 2(c), this central area clearly shows a reduction, and the complexity increases in the upper left corner. The same remodelling effect can be observed in figure 2(d), where the upper left area is already optimized, but cells in the lower right part show enhanced branching. This finding can be either attributed to different RGC subtypes which may vary in their outgrowth behaviour [36] or to variations in the growth cone dynamics, i.e. diverse phases of growth and collapse. Thus, the exact determination of the point in time when the network assumes a certain stage is complicated and will be discussed in the following section.

3.2. Quantification of network phases

A time-resolved analysis of the connectivity, shortest path length and edge length provides further insights into the evolving network. Therefore, network graphs were analysed in time steps of 90 min. In figure 3, the temporal development of the vertex number, connectivity, path length and edge length is given for the network shown in figure 2. All values are medians of the corresponding distributions. As expected, the number of vertices starts to increase up to a maximum value, which coincides in most of the cases with the most complex network. For several networks, we did not observe a sharp peak in the time dependence of the vertices but rather a plateau. Therefore, maximum and also optimized networks were judged by means of several criteria. Maximum networks were characterized by a high number of vertices combined with a large path length and a small edge length. After the simplification optimized networks were observed which are defined as networks that possess a reduced number of vertices and edges (see table 1), a decreased path length and a simultaneous increased edge length. These conditions were met as indicated in figure 3 by the red and blue arrows for the maximum and optimized network, respectively. As the networks formed, the connectivity of single vertices was found to increase from 1–2 from the initial network stage to 2–3 for maximum networks. It remained at the higher value for optimized networks, which is not surprising since neural networks aim at a high degree of connectivity. The shortest path length also increased, showing slight fluctuations until reaching the highest value for the maximum network. For all samples

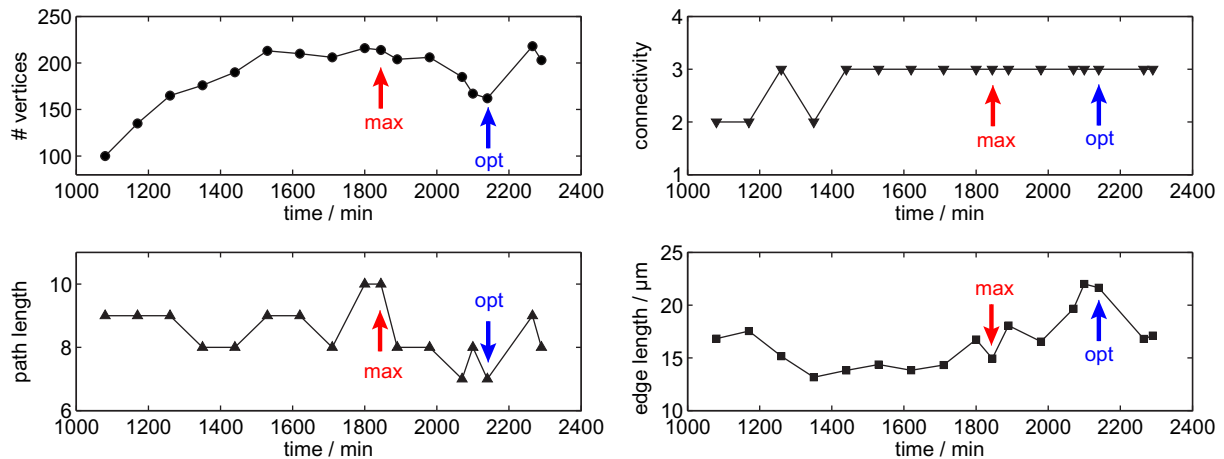


Figure 3. Temporal changes of the number of vertices, connectivity, shortest path length and edge length for the developing RGC network shown in figure 2. The network with maximum complexity and the optimized network were marked with red and blue arrows, respectively.

we found a reduction of the path length for the optimized network (see also figure 5). As mentioned above, at the stage of the maximum network, the system is characterized by many short segments. This is reflected by a decrease of the edge length to a minimum value. The restructuring of the network together with the observed straightening out of connections caused another growth of the edge length for the optimized network. The last two data points in figure 3 show a contrary trend for the number of vertices, path length and edge length. This behaviour has to be attributed presumably to the interplay of retraction and outgrowth, in this case the new outgrowth of neurites. However, the other networks did not show this trend. Thus, the quintessence about the differences between maximum and optimized networks was not affected.

Figure 4 shows the distributions of the connectivity, shortest path length and edge length for the network of figure 2 at prominent stages during the course of network formation, i.e. at the beginning of the observation (red), the maximum (blue) and the optimized network (green). The given values correspond to the median of the distributions. At the start, there are a large number of isolated cells or branching points and only a few vertices are connected (figure 4, top). Thus, we find that $k = 2$ for the median of the connectivity. For higher developed networks, i.e. the maximum and optimized networks, the number of neighbouring vertices increases to $k = 3$. This value is notably higher than the average connectivity of 2.38 reported for locust FGCs [9]. The connectivity distributions in the present study are more symmetric than those reported by Shefi and co-workers. Most remarkably, in the low connectivity wing, we found many fewer vertices with only one or two neighbours. In other words, especially the maximum and optimized mouse RGC networks were more connected than those of locust FGs. The connectivity was determined to be not scale-free. Although only undirected graphs were considered here, we did not see a power law distribution of the connectivity [37]. This is in agreement with other studies of (un)directed structural and functional neural networks [9, 38–40] as well as a graph-theoretic model [41]. A further aspect is the appearance of the connectivity distribution's long tail. High node degrees indicate the existence of hubs in the RGC networks which are characteristic of complex networks [42] and were also observed for other neural networks [10, 38, 43, 44].

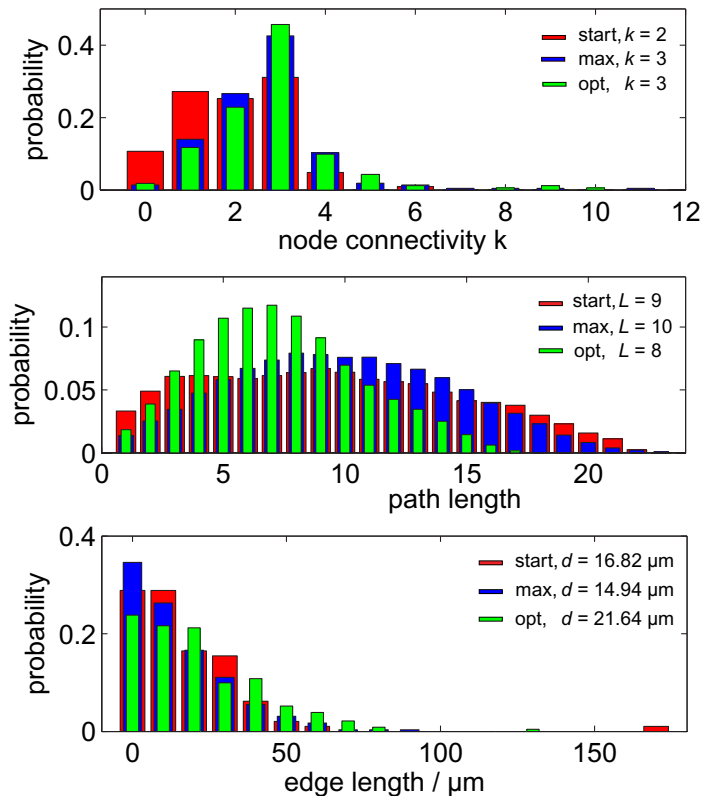


Figure 4. Distributions and medians of the connectivity, shortest path length and edge length resulting from the RGC networks shown in figure 2 at different stages of early network formation. Red: start of the observation (103 vertices, 101 connections); blue: maximum network (214 vertices, 273 connections); green: optimized network (167 vertices, 240 connections).

The path length distributions were found to be very broad for the initial and maximum networks (figure 4, centre). The largest path lengths observed ranged between 15 and 25, in a few cases maximum values of up to $L = 35$ were reached. As the network further evolved, there was a clear shift to shorter path lengths, which manifests in the path length's decrease of $14.53 \pm 3.39\%$ from the maximum to the optimized networks (see also figure 5). Averaged over all the optimized networks, we found $L_{\text{opt}} = 7.38 \pm 0.46$, which is less than half of the value reported earlier [9]. Thus, mouse RGC networks show significantly shorter path lengths than locust FGs *in vitro*, but are still larger than the average path length reported for *C. elegans*, macaque and cat cortex [3]. The large differences between these data probably result from the definition of vertices. Whereas for macaque and cat cortices the connectivity of whole clusters was analysed [45], in the case of *C. Elegans* single cells were counted as vertices [1]. In contrast, for 2D *in vitro* neuronal cultures the cell somata and neurite branching points were defined as vertices, which can cause larger path lengths (this work and [9]).

Edge length distributions for the striking stages are displayed in figure 4 (bottom). They reveal the existence of a large number of short edges ($d \leq 20 \mu\text{m}$) at the beginning of the network formation which is even exceeded in the maximum network. Most of the connections exhibited lengths between 10 and $70 \mu\text{m}$, although edge lengths up to $170 \mu\text{m}$ were observed at all stages during the network development. For optimized networks, the

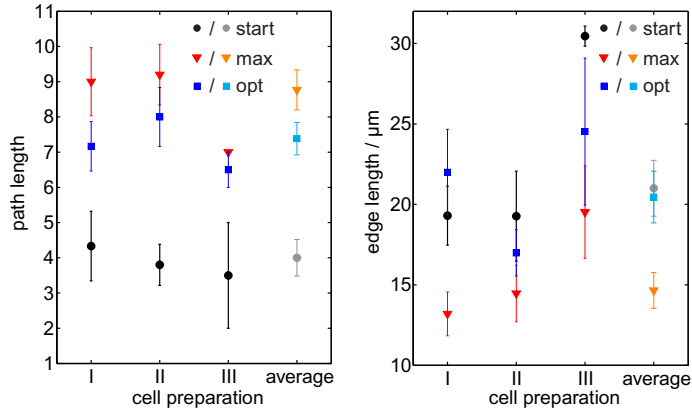


Figure 5. Shortest path length (left) and edge length (right) for RGC networks at the beginning of the observation (black circles), when the maximum network complexity is reached (red triangles) and for optimized networks (blue squares), respectively. The data correspond to three different cell preparations (including six, five and two networks, respectively) and the average over all samples. Error bars correspond to the standard error of the mean (SEM). Optimized networks are characterized by a reduced path length and an increased edge length.

edge length distribution shifted to higher values, i.e. for the edge length's median an average increase of $(45.16 \pm 11.98)\%$ from the maximum to the optimized network was found. This is attributed to the remodelling and simplification of the network accompanied by the observed straightening out of edges. Figure 5 presents the results for both the path length (left) and edge length (right) alterations of all 13 networks studied. The data clearly illustrate how these two parameters change at the pronounced stages of network formation. We observed a reduction of the average path length from $L_{\max} = 8.77 \pm 0.57$ to $L_{\text{opt}} = 7.38 \pm 0.46$ for optimized networks, which is accompanied by an edge length increase from $d_{\max} = (14.66 \pm 1.17) \mu\text{m}$ to $d_{\text{opt}} = (20.46 \pm 1.61) \mu\text{m}$. Our findings are consistent with earlier results from *C. elegans* and macaque cortex and structural human brain networks that were shown to favour a minimized path length (i.e. the number of processing steps) over an absolute minimum of the wiring length to maintain the high topological complexity of small-world networks [19, 46, 47].

3.3. Retinal ganglion cell networks are small-world networks

So far, we have focused on temporal changes of topological network parameters such as the connectivity, shortest path length, edge length and how RGCs evolve in different stages from a simple network to a system with an optimized architecture. However, networks are further characterized, essentially regarding the network class, by the clustering coefficient C and the so-called small-worldness S . The latter relates the small-world parameters C_{small} and L_{small} to corresponding values for random networks with the same number of vertices and edges and is given by $S = (C_{\text{small}}/C_{\text{rand}})/(L_{\text{small}}/L_{\text{rand}})$ [5]. Small-world networks stand out due to large cluster coefficients compared with random networks ($\overline{C}_{\text{small}} \gg C_{\text{rand}}$), where $C_{\text{rand}} \sim k/n$. Further, the path length L is much smaller than for regular graphs and similar to values for random graphs, i.e. $L_{\text{reg}} \gg L_{\text{small}} \geq L_{\text{rand}}$ with $L_{\text{reg}} = n/2k$ and $L_{\text{rand}} \sim \ln(n)/\ln(k)$ [1]. The

Table 2. Small-world parameters of three optimized RGC networks *in vitro* (n : the number of vertices, m : the number of edges, k : the median of connectivity, L : median of the path length, C : average clustering coefficient, S : small-worldness). The path lengths L_{reg} and L_{rand} and the clustering coefficient \bar{C}_{rand} of a regular and random network, respectively, with the same numbers of vertices, edges and connectivity are given for comparison.

n	m	k	L_{reg}	L	L_{rand}	\bar{C}	\bar{C}_{rand}	S
243	350	3	40.5	10	5.1	0.130	0.012	5.62
203	293	3	33.8	9	4.9	0.134	0.013	5.72
98	121	2	24.5	7	4.8	0.189	0.013	9.81

cluster coefficient averaged over all 13 RGC networks was determined to be 0.030 ± 0.011 at the beginning of the observation. As expected, when the networks evolved, the clustering coefficient increased to an average value of $\bar{C} = 0.095 \pm 0.013$ for both maximum and optimized networks. These results agree very well with locust FG *in vitro* networks [9] and are consistent with the results reported for connectivity patterns of *C. elegans* and zebrafish as well as different cortical networks [1, 3, 40].

For the largest network of each of the three cell preparations, the path lengths L_{opt} and the clustering coefficients C_{opt} are compared with corresponding values for regular and random networks, respectively (table 2). Therefore, ten random network graphs were generated using the Brain Connectivity Toolbox [6] and analysed as described above for the RGC data. All RGC networks exhibited path lengths that were much smaller than those of corresponding regular networks and slightly larger than L_{rand} . The clustering coefficients of RGC networks exceeded the values determined for analogue random networks by one order of magnitude. Finally, the small-worldness was found to be much larger than 1 for all three networks and was comparable with neural networks of *C. elegans* and macaque cortex or functional cortical connectivity of the human brain [5, 43, 46]. Very similar findings were obtained for maximum networks. Thus, our results show, on the one hand, that the studied mouse RGC networks (both maximum and optimized) form part of the family of neural small-world networks. On the other hand, we find that first the small-world architecture is established and subsequently optimized for short path lengths. Moreover, in complement to previous experience on complex networks achieved in invertebrate [9, 22] or using embryonic mix culture in rodent [10], our system using primary culture RGCs allowed us to develop an *in vitro* model of complex networks on postnatal neurons from the mammalian central nervous system. Discrepancies between the different models may help to understand why invertebrate or embryonic neurons are able to regenerate while mature neurons in mammals are not.

4. Concluding remarks

In this paper, we studied the formation of mouse RGC networks *in vitro* using time-lapse video microscopy and a time-resolved graph theoretical analysis. Although we let the neuronal networks form in a random way, the system self-organized to a non-random small-world network. During the early development of RGC networks, we identified different stages which

involved the reduction from a network with maximal complexity to an optimized network. At both stages, the networks displayed robust small-world properties. Network optimization was described as a property of small-world systems, but also for spatially constrained networks [7, 47]. In agreement with earlier results, we observed that evolving RGC networks do not exclusively strive for a large connectivity, but rather minimize the shortest path length for a high performance of information transmission [19, 46–48]. Thus, fundamental inherent neuronal properties reveal and govern the RGC outgrowth. These comprise, firstly, the formation of small-world networks which could be defined as the default programme for RGCs that are not in their natural environment and, secondly, the ability to optimize the network's architecture. In a future study, we aim to analyse the influence of external stimuli (namely glia signals, surrounding neuronal activity and chemoattractant molecules) on the modulation of those networks.

Acknowledgments

We thank the staff at the animal facility of the Faculty of Medicine (MEZ, University of Leipzig) for their excellent technical assistance and C A Naumann and P Rauch for support with the preparation of the tethered lipid bilayers. We also thank T Kießling, M Knorr, P Rauch and P Heine for their support with MATLAB and helpful discussions. This work was supported by the German foundation 'Stifterverband für die Deutsche Wissenschaft' and the French foundation 'Gueules Cassées' (to TC) and the DFG research unit 877 and the research training school 'Interneuro' (GK 1097; to LW).

References

- [1] Watts D J and Strogatz S H 1998 Collective dynamics of 'small-world' networks *Nature* **393** 440–2
- [2] Albert R and Barabási A 2002 Statistical mechanics of complex networks *Rev. Mod. Phys.* **74** 47–97
- [3] Boccaletti S, Latora V, Moreno Y, Chavez M and Hwang D 2006 Complex networks: structure and dynamics *Phys. Rep.* **424** 175–308
- [4] Strogatz S H 2001 Exploring complex networks *Nature* **410** 268–76
- [5] Humphries M D, Gurney K and Sporns O 2008 Network 'small-world-ness': a quantitative method for determining canonical network equivalence *PLoS ONE* **3** e0002051
- [6] Rubinov M and Sporns O 2010 Complex network measures of brain connectivity: uses and interpretations *NeuroImage* **52** 1059–69
- [7] Barthélemy M 2011 Spatial networks *Phys. Rep.* **499** 1–101
- [8] Varshney L R, Chen B L, Paniagua E, Hall D H, Chklovskii D B and Sporns O 2011 Structural properties of the *Caenorhabditis elegans* neuronal network *PLoS Comput. Biol.* **7** e1001066
- [9] Shefi O, Golding I, Segev R, Ben-Jacob E and Ayali A 2002 Morphological characterization of *in vitro* neuronal networks *Phys. Rev. E* **66** 21905
- [10] Downes J H *et al* 2012 Emergence of a small-world functional network in cultured neurons *PLoS Comput. Biol.* **8** e1002522
- [11] Sporns O, Tononi G and Edelman G M 2000 Theoretical neuroanatomy: relating anatomical and functional connectivity in graphs and cortical connection matrices *Cereb. Cortex* **10** 127–41
- [12] Sporns O, Chialvo D, Kaiser M and Hilgetag C 2004 Organization, development and function of complex brain networks *Trends Cogn. Sci.* **8** 418–25
- [13] Hilgetag C C and Kaiser M 2004 Clustered organization of cortical connectivity *Neuroinformatics* **2** 353–60

- [14] He Y, Chen Z J and Evans A C 2006 Small-world anatomical networks in the human brain revealed by cortical thickness from MRI *Cereb. Cortex* **17** 2407–19
- [15] Bullmore E T and Bassett D S 2011 Brain graphs: graphical models of the human brain connectome *Annu. Rev. Clin. Psychol.* **7** 113–40
- [16] Stam C 2010 Characterization of anatomical and functional connectivity in the brain: a complex networks perspective *Int. J. Psychophysiol.* **77** 186–94
- [17] Lago-Fernández L, Huerta R, Corbacho F and Sigüenza J 2000 Fast response and temporal coherent oscillations in small-world networks *Phys. Rev. Lett.* **84** 2758–61
- [18] Sporns O 2011 The human connectome: a complex network *Ann. Acad. Sci.* **1224** 109–25
- [19] Chen B L 2006 Wiring optimization can relate neuronal structure and function *Proc. Natl Acad. Sci.* **103** 4723–28
- [20] Bassett D S and Gazzaniga M S 2011 Understanding complexity in the human brain *Trends Cogn. Sci.* **15** 200–9
- [21] Honey C J, Thivierge J and Sporns O 2010 Can structure predict function in the human brain? *NeuroImage* **52** 766–76
- [22] Shefi O, Ben-Jacob E and Ayali A 2002 Growth morphology of two-dimensional insect neural networks *Neurocomputing* **44–46** 635–43
- [23] Bear M F, Connors B W and Paradiso M A 2007 *Neuroscience: Exploring the Brain* 3rd edn (Philadelphia, PA: Lippincott Williams and Wilkins)
- [24] Claudepierre T, Koncina E, Pfrieger F, Bagnard D, Aunis D and Reber M 2008 Implication of neuropilin 2/semaphorin 3F in retinocollicular map formation *Dev. Dyn.* **237** 3394–403
- [25] Steinmetz C C, Buard I, Claudepierre T, Nagler K and Pfrieger F W 2006 Regional variations in the glial influence on synapse development in the mouse CNS *J. Physiol.* **577** 249–61
- [26] Jordan R, Martin K, Räder H J and Unger K K 2001 Lipopolymers for surface functionalizations: 1. Synthesis and characterization of terminal functionalized poly(*N*-propionylethylenimine)s *Macromolecules* **34** 8858–65
- [27] Purrucker O, Förtig A, Lüdtko K, Jordan R and Tanaka M 2005 Confinement of transmembrane cell receptors in tunable stripe micropatterns *J. Am. Chem. Soc.* **127** 1258–64
- [28] Alker D, Harwood L M and Williams C E 1997 Carbamate derived stable precursors for generating chiral azomethine ylids under mild conditions *Tetrahedron* **53** 12671–78
- [29] Seitz P C, Reif M, Yoshikawa K, Jordan R and Tanaka M 2011 Dissipative structure formation in lipid/lipopolymer monolayers *J. Phys. Chem. B* **115** 2256–63
- [30] Cuntz H, Forstner F, Borst A, Häusser M and Morrison A 2010 One rule to grow them all: a general theory of neuronal branching and its practical application *PLoS Comput. Biol.* **6** e1000877
- [31] Brown K M *et al* 2011 The DIADEM data sets: representative light microscopy images of neuronal morphology to advance automation of digital reconstructions *Neuroinformatics* **9** 143–57
- [32] Hosseini S M H, Hoeft F, Kesler S R and Lambiotte R 2012 GAT: a graph-theoretical analysis toolbox for analyzing between-group differences in large-scale structural and functional brain networks *PLoS ONE* **7** e40709
- [33] Gleich D F 2009 gaimc: Graph algorithms in Matlab code (www.mathworks.com/matlabcentral/fileexchange/24134 MATLAB Central File Exchange, Retrieved 26 April 2012)
- [34] Bollobás B 1998 *Modern Graph Theory* (New York: Springer)
- [35] Kleder M 2005 Allspath www.mathworks.com/matlabcentral/fileexchange/8808-all-pairs-shortest-path-graph-solver MATLAB Central File Exchange, Retrieved 3 April 2012
- [36] Kim I, Zhang Y, Meister M and Sanes J R 2010 Laminar restriction of retinal ganglion cell dendrites and axons: subtype-specific developmental patterns revealed with transgenic markers *J. Neurosci.* **30** 1452–62
- [37] Amaral L A N 2000 Classes of small-world networks *Proc. Natl Acad. Sci. USA* **97** 11149–52
- [38] Sporns O and Zwi J D 2004 The small world of the cerebral cortex *Neuroinformatics* **2** 145–62
- [39] Perin R, Berger T K and Markram H 2011 A synaptic organizing principle for cortical neuronal groups *Proc. Natl Acad. Sci.* **108** 5419–24

- [40] Stobb M, Peterson J M, Mazzag B, Gahtan E and Hayasaka S 2012 Graph theoretical model of a sensorimotor connectome in zebrafish *PLoS ONE* **7** e37292
- [41] Humphries M, Gurney K and Prescott T 2006 The brainstem reticular formation is a small-world, not scale-free, network *Proc. R. Soc. B* **273** 503–11
- [42] Bullmore E and Sporns O 2009 Complex brain networks: graph theoretical analysis of structural and functional systems *Nature Rev. Neurosci.* **10** 186–98
- [43] Achard S 2006 A resilient, low-frequency, small-world human brain functional network with highly connected association cortical hubs *J. Neurosci.* **26** 63–72
- [44] Bonifazi P *et al* 2009 GABAergic hub neurons orchestrate synchrony in developing hippocampal networks *Science* **326** 1419–24
- [45] Hilgetag C, Burns G A P C, O’Neill M A, Scannell J W and Young M P 2000 Anatomical connectivity defines the organization of clusters of cortical areas in the macaque and the cat *Phil. Trans. R. Soc. B* **355** 91–110
- [46] Kaiser M and Hilgetag C C 2006 Nonoptimal component placement, but short processing paths, due to long-distance projections in neural systems *PLoS Comput. Biol.* **2** 805–15
- [47] Bassett D S *et al* 2010 Efficient physical embedding of topologically complex information processing networks in brains and computer circuits *PLoS Comput. Biol.* **6** e1000748
- [48] Bullmore E and Sporns O 2012 The economy of brain network organization *Nature Rev. Neurosci.* **13** 336–49